J. Magn. Soc. Jpn., **42**, 62-71 (2018)

<Paper>

Anisotropic Magnetic Core for the Iron Loss Reduction of Permanent Magnet Synchronous Motor

Nicolas Denis*, Shinya Takeda*, Kohei Fujitani*, Keisuke Fujisaki*, Shunya Odawara**

* Toyota Technological Institute, *2-12-1 Hisakata, Tempaku-ku, Nagoya 468-8511, Japan*

** Kitami Institute of Technology, *165 Koen-cho Kitami, Hokkaido 090-8507, Japan*

An interior permanent magnet synchronous motor (IPMSM) using a stator core made of grain-oriented (GO) anisotropic magnetic material is manufactured to evaluate the potential iron loss reduction that GO can bring compared to the conventionally used non-oriented (NO) quasi-isotropic silicon steel. The stator core is divided into yoke and teeth pieces that are arranged so that the GO material easy magnetization direction follows the main magnetic flux that flows in the core during the motor operation. The motor iron loss is measured under two conditions: 1) the IPMSM is rotated by an external motor ("drag force operation"), 2) the IPMSM is driven by a pulse-width modulation (PWM) inverter without load ("no-load operation"). The manufactured motor shows 13.5 % iron loss reduction during drag force operation and 5 % reduction during no-load operation. Numerical calculation is also carried out by 2-D finite element analysis (FEA) to confirm the experimental data.

Key words: Grain-oriented magnetic material, Iron losses, Magnetic core, Permanent magnet synchronous motor, Silicon steel

1. Introduction

Global warming and/or polluted urban areas is one of the biggest challenge that the society is facing today. Electrified vehicles are presented as one of the possible solutions but they still have to be more affordable and increase their autonomy in order to be more widely accepted by the society. The limited embeddable electrical energy in batteries is still a strong limit and therefore, the losses that occur in each part of the electrical powertrains should be reduced as much as possible. Interior permanent magnet synchronous motors (IPMSM) are known to be very efficient driving power sources for electrical vehicles but still contribute to waste of electrical energy caused by mechanical friction loss, coper loss and iron loss. In order to reduce the iron loss, focusing on the magnetic materials characteristics and applications is important [1].

Non-oriented silicon steel (NO) has small magnetic anisotropy. Moreover, its iron loss density and its magnetization characteristic are usually measured using the Epstein frame in which several sheets are superimposed with alternating direction (90°, 0°). In this way, the measured characteristic is considered as an average characteristic over the sheet orientation angle range. In other words, knowing the fact that the anisotropy is usually small, one single average characteristic is usually preferred for simplification rather that a complete characterization for every orientation angle. On the other hand, grain-oriented steel (GO) [2-3] has strong magnetic anisotropy [4] that has to be measured and characterized. GO is generally used for electrical transformer cores. It has very small iron loss density in its easy magnetization direction.

Fig. 1 shows the magnetic characteristics of NO and GO at 50 Hz taken from catalogue data [5]. The NO steel has one single characteristic, as explained previously, while the GO steel characteristic depends on the angle φ, which is the angle between the magnetic flux density vector and the easy magnetization direction. In particular, GO has low iron loss density in the easy magnetization axis ($\varphi = 0°$, (100) direction) while high in the transverse direction ($\varphi = 90°$, (010) direction).

Because the magnetic flux in a stator core of an electrical motor flows multi directionally, simply substituting NO steel by GO steel would make the magnetic flux force its way through the transverse direction of GO at some parts. This would have for consequence to likely increase the iron losses. This underlines the challenge of designing and manufacturing a motor core with GO steel. However, considering its superior magnetic properties, the authors think that GO is worth experimental trials in scientific research.

A proposed solution is to assemble the stator shifting each lamination from the previous one with a constant angle, so the easy magnetization direction appears in different parts of the stator [6]. This supposedly makes the magnetic flux pass from one lamination to another in order to avoid the parts which present the transverse magnetization direction. However, it can be argued that the magnetic flux could be restrained, causing a loss of performance of the motor. Moreover, in ref. 6), tests are done using the stator as a transformer core and not as part of an actual motor. Consequently, segmented type stators are tried in which teeth and yoke are divided [7-9], however only the teeth are made of GO steel. It would be interesting to evaluate the improvement of a stator composed solely of GO steel. GO steel is also applied to rotor cores [10-13] for which increase of electromagnetic torque and efficiency are reported. However, the rotor core is usually not the major contributor of the motor iron losses, so for the purpose of iron loss reduction, studies and trials should focus primarily on the stator.

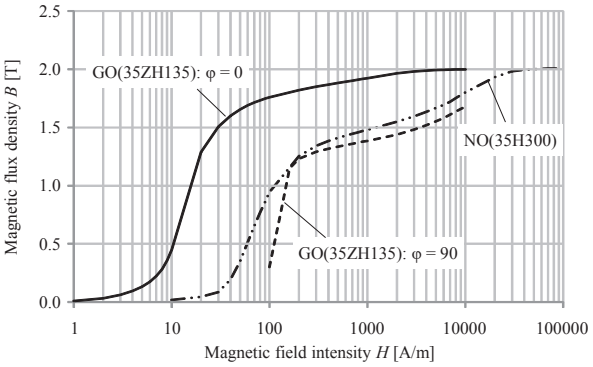

(a) *B-H* curve

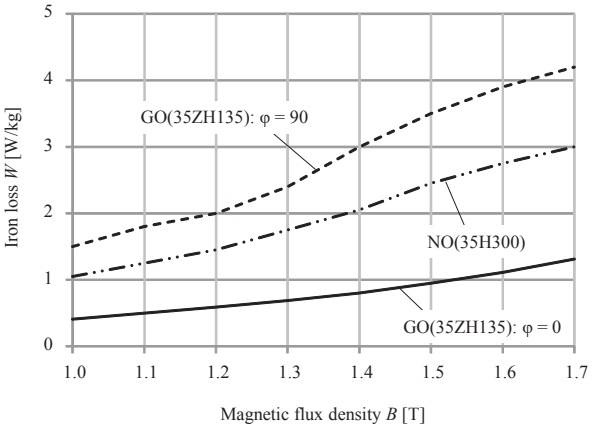

(b) *B-W* curve

Fig. 1 Magnetic characteristics of NO steel (35H300) and GO steel (35ZH135) at 50 Hz.

Considering the current state of the art described above, this paper proposes a novel assembly for an IPMSM stator core made completely of GO steel. The IPMSM using the proposed stator core, illustrated in Fig. 2, will be called "magnetic anisotropic motor" hereafter. The considerations lying under the proposed core assembly are as follows: at first, the assumption that the magnetic flux flows mainly in the radial direction in the stator tooth and in the tangential direction in the stator yoke is made. Based on this assumption, it is proposed to divide the yoke part and tooth part and cut GO steel pieces accordingly. The GO steel pieces are then arranged so that the GO easy magnetization direction coincides mostly with the tangential direction in the yoke and, similarly, the GO easy magnetization direction coincides mostly with the radial direction in the teeth. This configuration has been chosen as an attempt to maximize the correspondence between the magnetic flux direction and the GO easy magnetization direction. In previous works, the suitable shape of the proposed magnetic anisotropic motor was designed by using finite element analysis (FEA) [14]. Iron loss measurement trials have been made under "drag force operation" (IPMSM rotated by an external motor) in the previous work [15] but it is believed that these measurements along with the analysis have to be corrected and improved. Moreover ref. 15) does not present any results concerning the motor rotated by a pulse-width modulation (PWM) inverter, which is the most common way to drive an IPMSM.

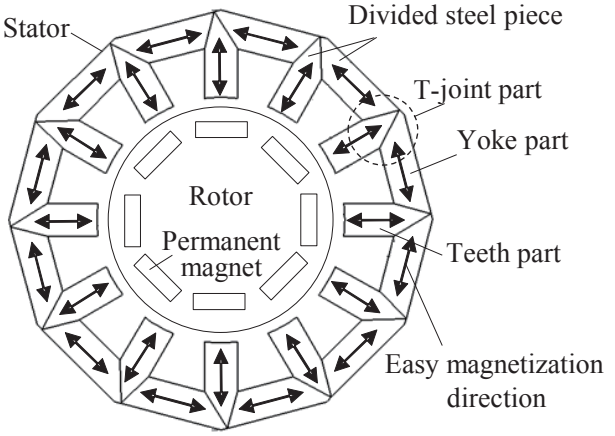

Fig. 2 Geometry of the proposed magnetic anisotropic motor.

In this paper, section II provides some important information about the manufacturing process. The manufacture of the stator core requires precision and limiting the mechanical stress as much as possible is crucial. In section III, the magnetic anisotropic motor is tested under both "drag force operation" and "no-load operation" (IPMSM driven by a PWM inverter without mechanical load) and its capacity to reduce iron loss is assessed. Finally, section IV presents numerical magnetic calculation to verify the measured data.

2. Trial Manufacture of Magnetic Anisotropic Motor

The GO steel 35ZH135 is used to manufacture the stator of an IPMSM with 12-slots, 8-poles, and concentrated windings. The detailed geometry is shown in Fig. 3 and Table I. In the proposed geometry, the slot opening is quite large and will cause a high torque ripple. Since no dedicated machinery was available to wind the stator, wide slot opening has been chosen to make the winding process easier to do by hand. Since the reduction of torque ripple is not the focus of this study, it is considered that this particular geometry does not negatively affect the conclusions of this paper.

For the sake of comparison, a stator made of NO steel 35H300 has also been manufactured. Since the manufacture process of the NO stator is significantly different from that of the GO stator, it is difficult to obtain geometrical similarity to the 10 microns order. The dimensions of the NO stator differ slightly from Table I. R_{Si} is equal to 38.20 mm and the axial length to 46.9 mm. It is thought that the differences observed do not influence the iron loss to the point at which a comparison is significantly unfair.

In both cases, the rotor core of the motor is made of NO steel (35H300). Sintered NdFeB permanent magnets (PM) are used. Their characteristics are given in Table II.

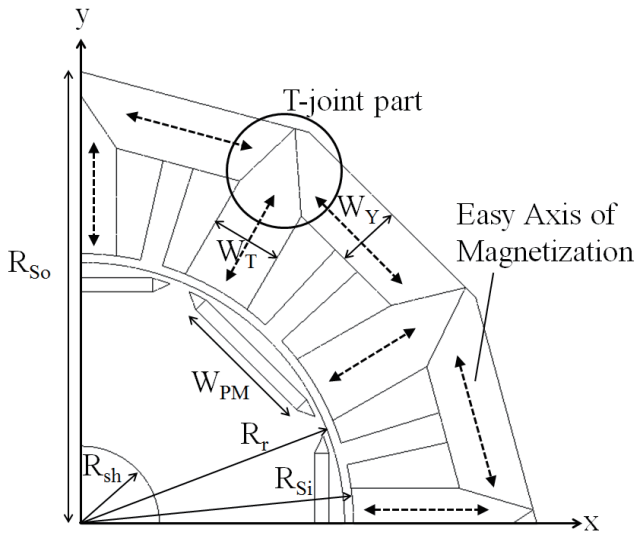

Fig. 3 Proposed magnetic anisotropic motor (quarter size model).

TABLE I SPECIFICATIONS OF MAGNETIC ANISOTROPIC MOTOR.

Number of poles	-	8
Number of slots	-	12
Radius of stator core (outside)	R_{So}	64 mm
Radius of stator core (inside)	R_{Si}	38.15 mm
Yoke width	W_Y	9.17 mm
Teeth width	W_T	10.00 mm
Radius of rotor	R_R	36.95 mm
Air gap between stator and rotor	G	1.20 mm
PM width	W_{PM}	20 mm
Stator axial length	-	47.0 mm
Winding method	-	Concentrated

In the GO stator core, the junction between the tooth part and the yoke parts is illustrated in Fig. 4. A joint structure without overlap from one layer to another, as in Fig. 4.a, would cause mechanical brittleness. Consequently, a structure with overlaps, as in Fig. 4.b, has been chosen to ensure the stator overall solidity. Therefore, the angle θ defined in Fig. 4.b has to be taken inferior to 90°. In the previous study [14], numerical analysis has been performed in order to find an angle θ that would ensure good tradeoff between iron loss minimization and mechanical solidity. The selected angle is 80°.

The manufacture process of the GO stator has been detailed in previous papers [14)-15)]. This paper does not aim at providing detailed manufacture explanations but some points should be noted. For both the GO and NO stators, wire electric discharge machining has been used to cut the electrical steel sheets while avoiding high mechanical stress [16)]. In order to improve the mechanical solidity of the GO stator, compressive force was applied for 30 minutes after each completed layer. As a consequence, the stacking factor of the GO stator is slightly higher (99.8%) than for the NO stator (97.7%). GO is known to have more stress sensitivity than NO

TABLE II CHARACTERISTICS OF PERMANENT MAGNETS AT ROOM TEMPERATURE.

PM residual magnetization	B_m	1.28 T
Coercive force	H_c	1.02×10^6 A/m
Electrical conductivity	σ	6.25×10^5 S/m

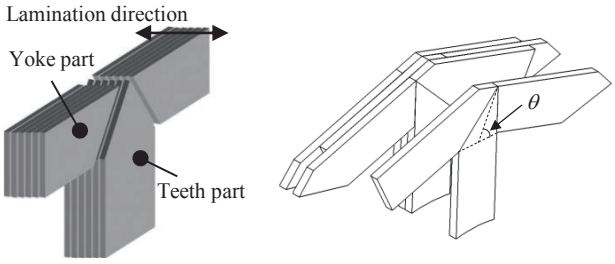

(a) No overlapping (b) Overlapping

Fig. 4 T-joint part, (a) No overlap, (b) With overlap.

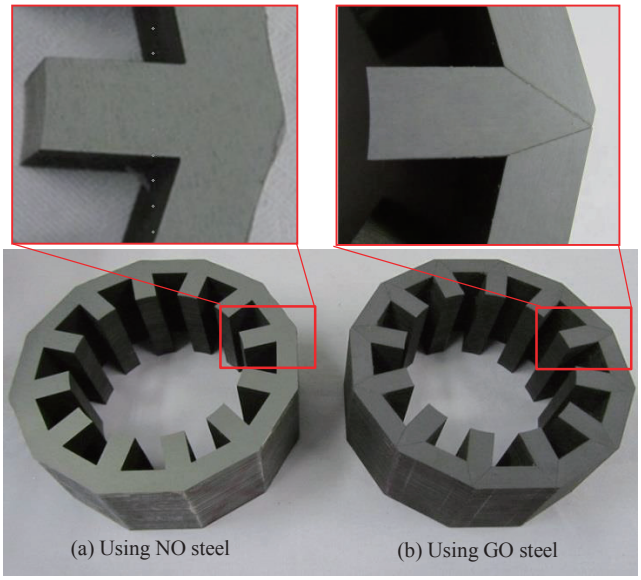

Fig. 5 Completed stator core specimens.

but the effect is negligible in case of uniform axial compression. Therefore, a jig[15)], which was manufactured so that a good geometrical accuracy can be kept, is prepared to avoid this type of stress. Fig. 5 shows the completed stator core specimens.

It can be understood that the GO requires extra manufacture because of the special junction between teeth parts and yoke parts. On top of that, GO requires more cutting using the rather expensive wire electric discharge machining. Therefore, the proposed GO stator core increases manufacture complexity and cost, which is a disadvantage compared to the NO stator. However, future development in manufacturing technology could help to overcome these problems. Moreover, as motor applications expand widely, the proposed GO stator core could be useful for special applications (like aircraft or spacecraft) in which the iron loss reduction is required while the motor core cost is less crucial.

3. Experimental Evaluation of Magnetic Anisotropic Motor

As explained in the introduction, the manufactured magnetic anisotropic motor iron losses are evaluated experimentally under "drag force operation" and "no-load operation". Table III shows equipment used for the operations. The tests are explained hereafter.

3.1 Drag Force Operation

The drag force operation measurement system is illustrated in Fig. 6. No current is supplied to the tested IPMSM (trial motor MS). The rotor of the IPMSM is rotated by an external brushless DC (BLDC) motor. The BLDC motor rotational speed ω and output torque T are measured by a revolution indicator and a torque meter, respectively. When the rotor is rotated by the BLDC motor, the rotating permanent magnets magnetize the stator core, which creates stator iron losses. The teeth shape of the IPMSM stator core generates variating magnetic flux density in the rotor and magnets which cause rotor and magnet iron losses.

Since no electrical power is supplied to the IPMSM, the output power supplied by the BLDC motor balances all the IPMSM losses, namely the iron loss W_{i_drag} and the mechanical friction loss W_m. Then the following equation holds.

$$P_{out} = \omega T = W_{i\_drag} + W_m, \quad (1)$$

where P_{out} is the BLDC motor output mechanical power.

In order to measure the mechanical loss, a rotor with demagnetized permanent magnets is used. It has the same shape and bearings as the rotor with magnetized permanent magnets. When the same drag force test as described above is carried out replacing the conventional rotor by the demagnetized rotor, there are no iron loss generation and the term W_i disappears in (1). Therefore, W_m can be calculated using the following equation.

$$P'_{out} = \omega T' = W_m, \quad (2)$$

where P'_{out} and T' are the BLDC motor output mechanical power and torque respectively, when the demagnetized rotor is used. The IPMSM iron losses under drag force operation can be deduced from (1) and (2).

The torque to measure is relatively small, which makes the measurements more susceptible to uncertainties. The torque meter chosen for the test can measure a maximum torque of 1 N·m and has an accuracy of ±2 mN·m, which corresponds to ±0.157 W at 750 rpm and ±0.628 W at 3000 rpm for the measured power accuracy. In order to improve the reliability of the results, the motor runs a first for 30 minutes at a given speed in order to reach thermal steady-state operation and avoid measurement differences due to thermal transient behavior. Then one measurement consists in recording the torque and speed for 20 seconds. The recorded data are then averaged over the 20 seconds time span. This procedure is done 10 times. The standard deviation of the 10 measurements is then calculated.

3.2 No-load Operation

During no-load operation, the trial IPMSM is driven by a 3-phase PWM inverter. As shown in Fig. 7, the inverter output power $P_{inverter}$ and the IPMSM phase RMS current I_n are measured using a power analyzer whose bandwidth is 2 MHz and sampling frequency 2.2 MHz. The rotational speed is controlled using a vector control scheme and a speed feedback provided by an encoder. The d-axis IPMSM phase current reference is set to zero, the PWM carrier frequency to 1 kHz and the DC bus voltage to 180 V.

Because the trial IPMSM has no mechanical load, the power balance verifies the following equation.

$$P_{inverter} = 3R_a I_n^2 + W_m + W_{enc} + W_{i\_inv}, \quad (3)$$

where R_a (0.510 Ω) is the phase resistance that has been measured in DC condition just after the measurements, W_{enc} is the mechanical loss of the encoder measured by the same method as used for the estimation of W_m. Then the IPMSM iron loss under no-load operation W_{i_inv} can be deduced.

The measurement procedure of ten consecutive trials introduced in the last section has also been carried out to increase the reliability of the measurements.

TABLE III EXPERIMENTAL EQUIPMENT.

Item	Model	Manufacturer
Torque meter	TH-3014H	Ono Sokki
Revolution indicator	MD-0118	Ono Sokki
Watt meter	TS-2800	Ono Sokki
Blushless DC motor	BXM6200-A	Oriental motor
Encoder	MES-20-1024	Microtech Laboratory
Power analyzer	PPA-5530	Iwatsu
PWM inverter	MWINV-9R122B	Myway Plus

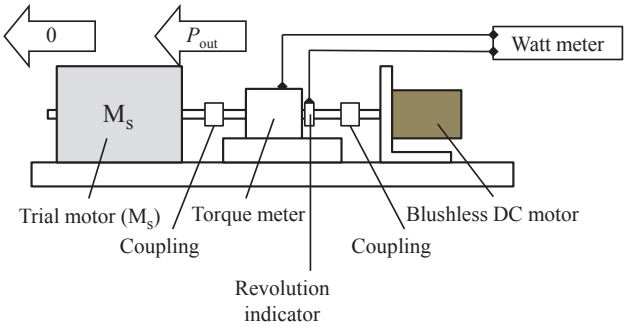

Fig. 6 Schematic diagram of the iron loss measurement system by drag force test.

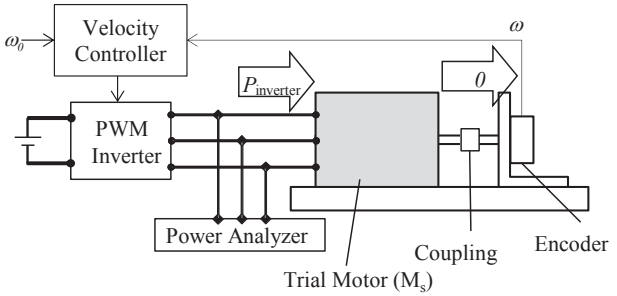

Fig. 7 Schematic diagram of the iron loss measurement system by no-load test.

3.3 Measurement Results of Drag Force Test

The IPMSM iron loss is measured at 750 rpm, 1500 rpm, 2250 rpm and 3000 rpm which correspond to an electrical fundamental frequency of 50 Hz, 100 Hz, 150 Hz and 200 Hz respectively. The results obtained for both IPMSMs (with GO stator and with NO stator) are shown in Fig. 8. The bars represent the standard deviation of the ten measurements. The iron loss reduction calculated considering the average of the ten measurements is also presented in Fig. 8. Even though the reduction could be considered small given the increased manufacture complexity, a reduction is observed and is considered to be due to the superior characteristics of GO steel [17] and the laser scratch that downsizes the magnetic domains and then reduce the excess loss [18].

3.4 Measurement Results of No-load Test

The iron losses measured under no-load operation are illustrated in Fig. 9. As in the previous section, the standard deviation of the ten measurements is also illustrated using bars. The PWM inverter causes high order harmonics in the magnets, rotor and stator magnetic flux that contribute to increase the iron loss compared to drag force operation [19)-20)]. Under PWM inverter excitation also, it appears that the GO stator decreases the IPMSM iron loss. However, the reduction percentage is smaller compared to the drag force condition, especially at 750 rpm (50 Hz). This can be explained by the fact that the GO material is originally intended for application at 50/60 Hz and has its best reduction potential at these frequencies compared to NO. At higher frequencies, the iron loss density reduction worsens, as shown by Table IV.

4. Analysis of Magnetic Anisotropic Motor

The measured iron loss data need to be confirmed by numerical calculation. Here, a 2-dimensional (2-D) model for magnetic field analysis and Steinmetz equations for iron loss calculation are used. Some assumptions and simplifications are made and detailed in the following sections, along with their possible consequences. It should be noted that the aim of this paper is to evaluate the potential gain of using GO steel in the proposed configuration and numerical analysis is done to confirm the experimental data. Since the final purpose of the paper is not to propose a novel numerical model, it is considered that the simplifications and assumptions could lead to possible inaccuracies but are acceptable given the targeted purpose.

4.1 Method for Magnetic Field Analysis

The 2-D model is based on FEA with A-method used as in ref. 21). The fundamental equation is expressed as follows:

$$\frac{\partial}{\partial x}\left(v_y \frac{\partial}{\partial x} A_z\right)+\frac{\partial}{\partial y}\left(v_x \frac{\partial}{\partial y} A_z\right) = -J_0+\sigma \frac{\partial}{\partial t} A_z - v_0 \frac{\partial}{\partial x} M_y + v_0 \frac{\partial}{\partial y} M_x \quad (4)$$

where A_z is the vector potential on the z-axis, v_x and v_y are the magnetic reluctivity on the x and y axis, v_0 is the space magnetic reluctivity, J_0 is the current density supplied to the coil parts, σ is the electrical conductivity of the material, and M is the magnetization of permanent magnets.

In the GO stator, two-axis anisotropic method is used to model the magnetic anisotropy. It provides satisfactory magnetic field analysis when the material is not magnetically saturated [22)]. The magnetic reluctivity v_x is the reluctivity of GO in the easy magnetization axis and v_y is the reluctivity in the transverse magnetization axis. They are calculated from Fig. 1.a. Since the easy axis and transverse axis direction change at each tooth and yoke part, it is impossible to take a unique (x, y) reference frame for the whole numerical model. Consequently, each tooth or yoke part has its own reference frame.

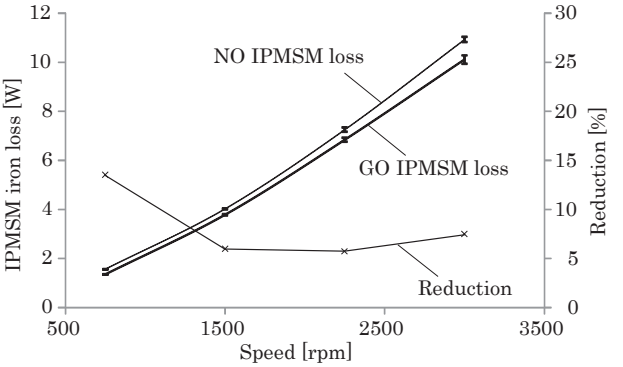

Fig. 8 Iron loss comparison between magnetic anisotropic motor and IPMSM with NO stator core under drag force operation.

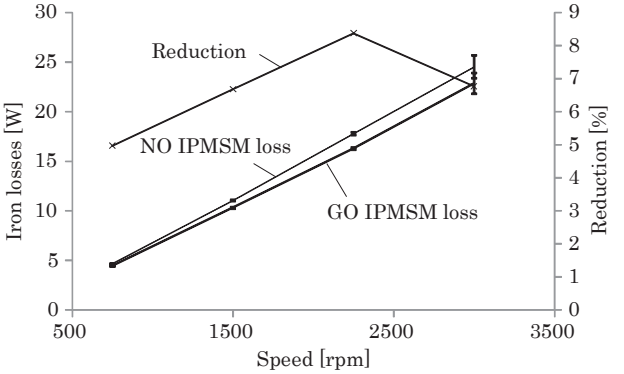

Fig. 9 Iron loss comparison between magnetic anisotropic motor and IPMSM with NO stator core under no-load operation.

TABLE IV MATERIAL IRON LOSS DENSITY OF NO (35H300) AND GO (35ZH135) AT B= 1 T.

Exciting frequency (Hz)	50	100	200	1000
NO (W/kg)	1.06	2.54	6.59	77.8
GO easy magnetization direction (W/kg)	0.415	1.25	3.90	64.1
Reduction ratio (%)	60.9	51.0	40.8	17.6

Similarly to the Epstein frame configuration explained in the introduction, the NO stator lamination is done by stacking the cut sheets with different orientation angles (made possible by the several symmetries of the stator shape). In this way, the stator has small local anisotropy but can be considered to have a global magnetic isotropy since the material orientation angle differs through the stator axial length, covering the whole angle range. As a consequence, it is possible to use a single average *B*-*H* characteristic in the FEA model without causing large inaccuracies. In other words, ν_x and ν_y are considered equal in (4) for the model of the NO stator.

Because of the interlamination insulation and the fact that a 2-D model is used, the electrical conductivity is taken null in the stator and rotor. The magnetic field induced by the eddy current is not considered and the eddy current losses are approximated by using the Steinmetz equations. The electrical conductivity of permanent magnets however is considered and the magnets eddy current losses are obtained from the calculation of the eddy currents flowing in the magnets. Moreover, the magnetic reluctivity of the magnets is taken equal to that of the air.

When simulating the drag force operation, J_0 is taken null since there is no current in the coils. When simulating the no-load operation, the phase current that has been measured during the no-load tests are used as input of the numerical model. In other words, the current density J_0 is calculated based on the measured phase current.

To evaluate the iron loss density W_{GO} in the GO stator, the magnetic flux density is first decomposed into its components in the easy magnetization direction B_e and the transverse magnetization direction B_h. In this way, the decomposition of the magnetic flux density vector depends on the part (yoke or tooth) that is considered. A fast Fourier transform (FFT) is then performed to find the harmonic components of B_e and B_h [23]. Finally, the iron loss density at each point is calculated using the Steinmetz approximation [24)-25)].

$$W_{GO} = \sum_{i=1}^{N} \{(K_{hys,e,i} B^2_{e,i} + K_{hys,h,i} B^2_{h,i}) f_i + (K_{ed,e,i} B^2_{e,i} + K_{ed,h,i} B^2_{h,i}) f^2_i\} \quad (5)$$

where i is the harmonic rank, N is the rank of the highest harmonic, f_i is the frequency of the i^{th} harmonic, and $B_{h,i}$ and $B_{e,i}$ are the amplitudes of the i^{th} harmonic of B_h and B_e respectively. $K_{hys,e,i}$ and $K_{hys,h,i}$ are the hysteresis loss Steinmetz constants of the GO in the easy and transverse magnetization directions respectively. $K_{ed,e,i}$ and $K_{ed,h,i}$ are the eddy current loss Steinmetz constants of the GO in the easy and transverse magnetization direction respectively.

As the NO stator is considered to have global magnetic isotropy, the following equation can be used instead of (5) for the calculation of the iron loss density.

$$W_{NO} = \sum_{i=1}^{N} \{K_{hys,i} (B^2_{t,i} + B^2_{r,i}) f_i + K_{ed,i} (B^2_{t,i} + B^2_{r,i}) f^2_i\} \quad (6)$$

where unlike (5), the magnetic flux density is decomposed into its radial B_r and tangential B_t components and the Steinmetz constants do not depend on the direction in the material as shown by the disappearance of the index h and e. The Steinmetz constants depend on the frequency as shown by the index i, and are calculated using the "two-frequencies method". This method, illustrated in Fig. 10, is basically an interpolation using the material iron loss characteristics of Fig. 11. Figure 10 illustrates the case of NO but the same procedure is applied to GO for both the easy and transverse magnetization directions. The interpolation is done by considering the two available nearest frequencies to the frequency f_i.

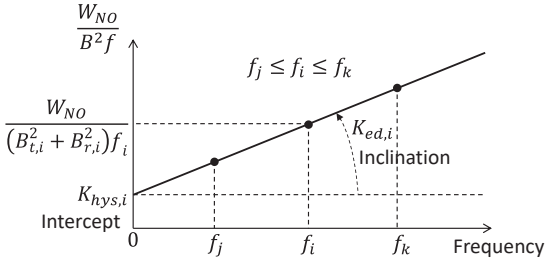

Fig. 10 Two-frequencies method to calculate the Steinmetz constants.

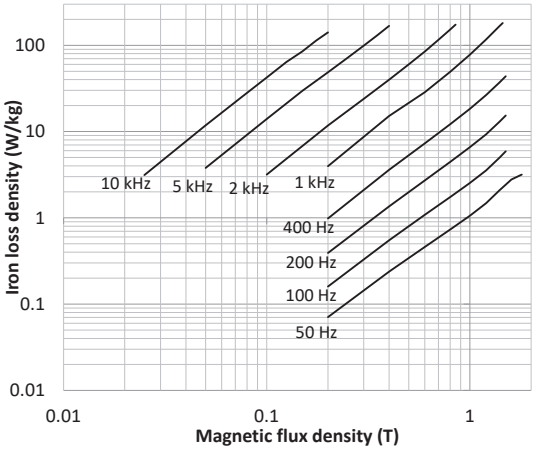

(a)

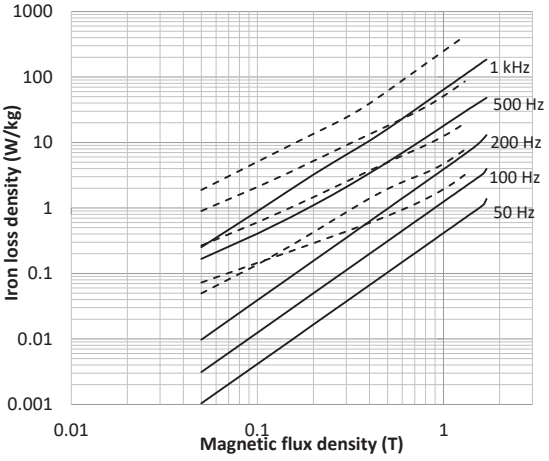

(b)

Fig. 11 Material iron loss density characteristics of GO and NO. (a) 35H300 (b) 35ZH135 easy magnetization direction (solid curve) and transverse direction (dashed curve).

Equations (5) and (6) are a sum through the harmonics of the magnetic flux density [26]. The harmonics in the stator magnetic flux caused by the rectangular magnets, the harmonics in the magnet and rotor magnetic flux caused by the stator slots, and the harmonics caused by the PWM inverter are taken into account in the calculation of the motor iron losses [27].

Moreover, even though the 2-D components of the magnetic flux density are considered in (5) and (6), the additional iron loss due to the rotation of the magnetic flux [28] is not modeled in this paper. For more accuracy, modeling the impact of rotational magnetic flux on the iron loss is preferable. However, for the NO material, previous works show that the approximation (6) results in a relatively good agreement between experiment and calculation [27),29]. As for the GO material, the permeability in the transverse direction is much lower than in the easy magnetization direction. Therefore, the question of whether or not the magnetic flux is rotating in the GO stator remains to be investigated at this stage. It is proposed to do this investigation for the case of drag force operation at 750 rpm. Through magnetic flux analysis, the magnetic flux density locus is calculated at three different points of the stator shown in Fig. 12. The magnetic flux density locus presents the variations of the components B_e and B_h of the magnetic flux density simultaneously through one electrical period. Fig. 13 shows the obtained results. It can be seen that for all points, the magnetic flux is stronger in the easy magnetization direction but the component in the transverse direction remains non-negligible, especially in the tooth part, showing that the magnetic flux is rotating. In order to confirm that, it is proposed to illustrate the magnetic flux lines at a given position of the rotor. The flux lines are shown in Fig. 14. It can be seen that some flux lines in the stator tooth are in the transverse direction especially when the tooth faces the space between two magnetic poles. Based on these observations, it is acknowledged that the impact of the rotational magnetic flux on the GO iron loss should be investigated in order to improve the model accuracy. Since it is a quite difficult task, this study is left for future work.

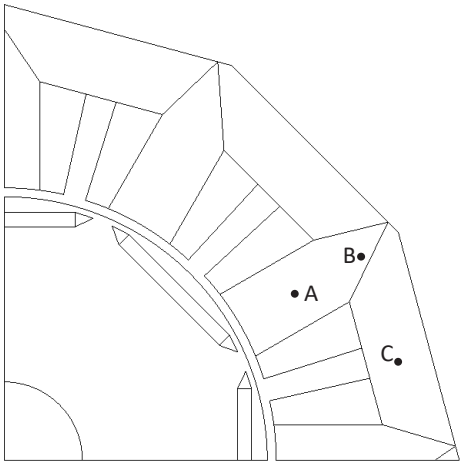

Fig. 12 Points considered for the investigation of the magnetic flux density locus.

Finally, the stator made of GO steel has much more cutting than the stator made of NO steel. It is known that cutting an electrical steel sheet increases the iron loss density in the vicinity of the cutting line. In this paper, wire electric discharge machining has been used for cutting. The paper does not aim at quantifying the impact of the cutting on the GO stator iron losses but it should be noted that wire electric discharge machining causes very low level damage and can even leave the material undamaged when the process is followed by stress relief annealing under nitrogen atmosphere at 820 °C for 3 hours [16]. It is then assumed that the damaged area will have only a small impact on the actual motor iron losses and consequently, the choice has been made not to model them in the FEA for a matter of simplification.

4.2 Influence of the Clearance Between the stator Pieces

The manufacture process of the GO stator results in a small clearance between the yoke and teeth pieces. The magnetic flux analysis results illustrated in the previous section is obtained using a finite element model that ignores the clearance.

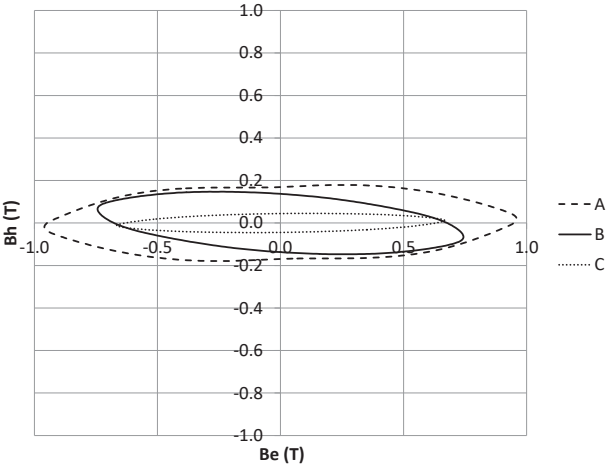

Fig. 13 Magnetic flux density locus in the GO stator obtained by FEA (drag force operation at 750 rpm).

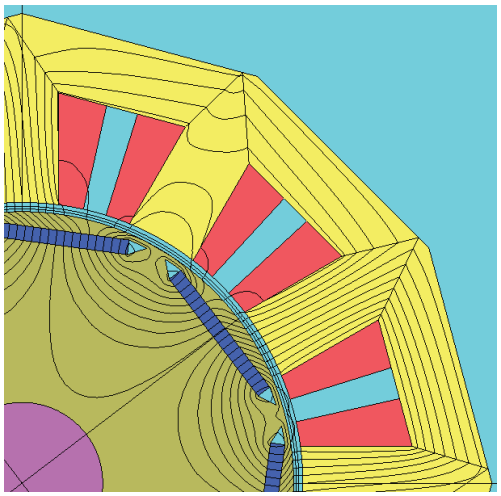

Fig. 14 Magnetic flux lines in the magnetic anisotropic motor (drag force operation at 750 rpm).

As a first approximation, it can be said that the total

reluctance of the magnetic flux path is mainly determined by the rotor/stator air gap plus the magnet and that the small clearance does not impact the total reluctance significantly. In this section it is proposed to evaluate the influence of the clearance on the stator magnetic flux density and iron losses.

If one considers a space factor of 98% in a laminated core of 350 µm thick steel sheets, it makes an interlamination of approximately 7 µm. The assembly of yoke and tooth parts has been done using an accurate jig [15] that ensures similar clearance between pieces while limiting mechanical pressure in the lamination direction. The clearance is then likely to be larger than 7 µm and slightly different at each junction. Choosing a representative clearance seems to be difficult but considering the above points, a model with a clearance of 10 µm is developed. Moreover, considering the tight clearance, unevenness due to imperfect cutting might locally affect the magnetic flux density. Because of the difficulty of modeling the unevenness of the air gap, the clearance has been chosen uniform through the whole gap in the new model.

The magnetic flux density locus obtained with the new model is illustrated in Fig. 15. The pieces clearance changes the magnetic flux density quite sensibly, especially in the T-joint part (point B), compared to the case in which there is no clearance (Fig. 13).

Table V gives the results of the IPMSM iron losses calculation using both models (with and without pieces clearance). Simulation results for both drag force and no-load operations at 750 rpm are presented. It can be seen that the iron losses are slightly lower when the clearance is included but the results remain close. Considering the above observations, it is decided to keep the model including pieces clearance for all the simulations whose results are presented in the next section.

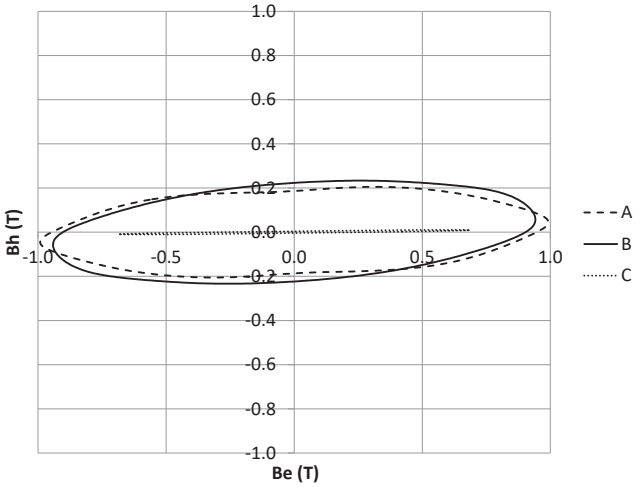

Fig. 15 Magnetic flux density locus in the GO stator obtained by FEA considering the pieces clearance (drag force operation at 750 rpm).

4.3 Calculation Results

Fig. 16 and Fig. 17 show the measurements and the numerical analysis results of both magnetic anisotropic and NO IPMSMs iron losses in drag force and no-load conditions respectively. For both numerical analysis and experiments, the magnetic anisotropic IPMSM has lower iron losses than the NO IPMSM.

TABLE V IRON LOSS CALCULATION RESULTS OBTAINED BY 1) MODEL CONSIDERING PIECES CLEARANCE, 2) MODEL WITHOUT PIECES CLEARANCE (750 RPM)

		No clearance [W]	With clearance [W]
Drag force	IPMSM total iron loss	1.53	1.49
	Stator loss	1.134	1.095
	Rotor loss	0.356	0.353
	Magnet loss	0.0408	0.0391
No-load	IPMSM total iron loss	2.86	2.81
	Stator loss	1.250	1.212
	Rotor loss	0.526	0.521
	Magnet loss	1.086	1.077

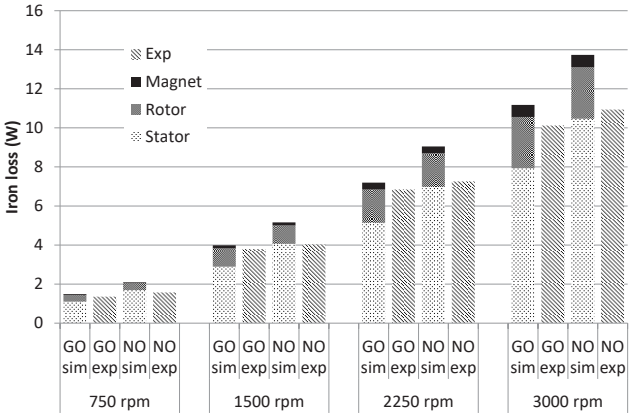

Fig. 16 Numerical analysis and measurements of IPMSM iron losses in drag force condition.

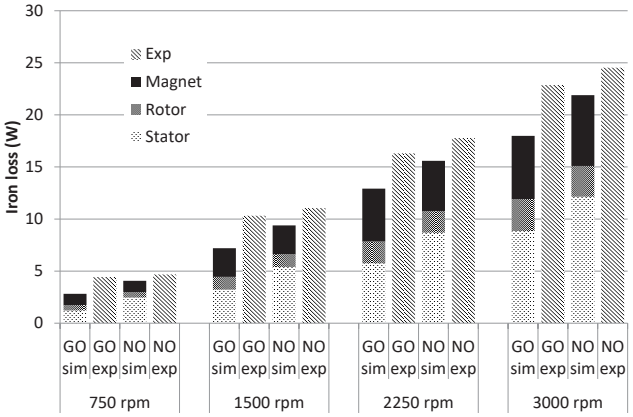

Fig. 17 Numerical analysis and measurements of IPMSM iron losses in no-load condition.

However, the iron loss difference between the magnetic anisotropic motor and the NO IPMSM is larger for the numerical calculation than for the experiments. In particular, at 3000 rpm for example, the measurements show a decrease of total iron losses by about 7.5 % in drag force condition and 6.8 % in no-load condition. In comparison for the same speed, FEA results show that the magnet and rotor iron losses are very similar for both motors but the stator iron losses drop by about 24 % in drag force operation and 27 % in no-load operation when the GO stator is used. As explained in section 4.1, the rotational losses have not been taken into account in the FEA neither for the NO IPMSM nor the magnetic anisotropic motor. It is thought that the rotational magnetic flux density in the GO material may have a bigger impact than for the NO material, which could explain the lower iron loss decrease obtained by experiment. Moreover, both experiment and numerical calculation show an increase of iron losses between the drag force and the no-load operations. This is due to the high frequency voltage supplied to the motor coils by the PWM inverter in no-load condition [19)-20)]. The magnet eddy currents are especially strongly affected [30)].

The peak magnetic flux density and the iron loss distributions calculated by FEA for drag force operation at 750 rpm are presented in Fig. 18 and Fig. 19 for the NO IPMSM and the magnetic anisotropic motor respectively. It should be noted that the iron loss distribution shows only the rotor and stator iron losses but not the magnet eddy current losses because both are made at different calculation steps. In the NO IPMSM the magnetic flux flows from the tooth to the yoke concentrated in the inner area and the magnetic flux density in the outer of the tooth/yoke junction area remains low. Comparatively, for the magnetic anisotropic motor, the magnetic flux rotates less and remains as much as possible in the easy magnetization direction. Therefore it flows all the way towards the outer of the T-joint area, resulting in a higher iron loss density compared to the NO stator in this zone. Everywhere else, the iron loss density in the GO stator is smaller than in the NO stator. For both motors, the peak magnetic flux density in the tooth is higher than in the yoke, which results in higher iron loss density. The difference of iron loss density between the tooth and yoke parts seems to be more accentuated in the GO stator though. This can be explained by the fact that, besides the higher peak magnetic flux density, the magnetic flux density component in the transverse direction is larger in the tooth part than in the yoke part (Fig. 15).

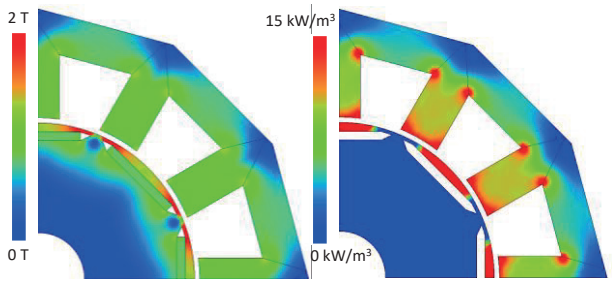

(a) Magnetic flux density (b) Iron loss density

Fig. 18 Peak magnetic flux density and iron loss density distributions of NO IPMSM at 750 rpm (drag force operation).

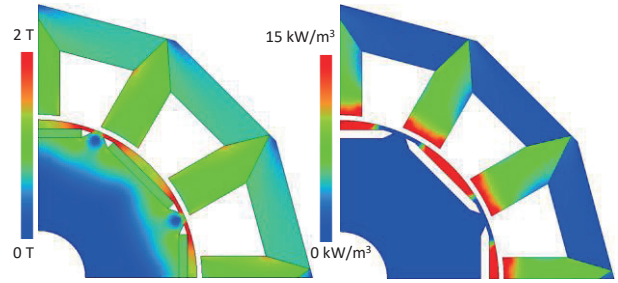

(a) Magnetic flux density (b) Iron loss density

Fig. 19 Peak magnetic flux density and iron loss density distributions of magnetic anisotropic motor at 750 rpm (drag force operation).

5. Conclusion

A novel permanent magnet synchronous motor using a stator made of grain-oriented steel sheets has been evaluated. In drag force test conditions at 750 rpm, the experiments show that the iron losses of the proposed motor are 13.5 % lower than the iron losses of its equivalent motor using exclusively non-oriented silicon steel. The reduction becomes 5 % in no-load condition at 750 rpm.

The GO stator requires more cutting than a conventional stator and a low damage cutting technique is preferred knowing the sensitivity of GO to mechanical stress. Consequently, even though GO can reduce the motor iron losses, the GO stator manufacture is more costly, making it more suitable for special applications like aircrafts or spaceships at this moment. Moreover, numerical analysis could be improved by taking rotational losses and cutting damage into account. Finally, a simple geometry has been chosen for the stator core proposed in this paper. Thus, further optimization is still a possible future investigation in order to fully benefit from the characteristics of the GO material.

Acknowledgements This research is partially supported by KAKENHI (26420259) of Ministry of Education, Culture, Sports, Science and Technology.

References

1) K. Fujisaki: "Future Magnetic Material Property Installed in and Driven by Power Electronics Technology," *IUMRS-ICAM 2015 (14th Int. Union Materials Res. Soc. – Int. Conf. Adv. Materials)*, IV-1Th3F1-1 (IS), 2015.10.29.
2) N. P Goss: "Electrical sheet and method and apparatus for its manufacture and test," *U.S. Patent 1965559*, 1934.
3) S. Taguchi, T. Yamamoto, and A. Sakakura: "New grain-oriented silicon steel with high permeability "ORIENTCORE HI-B"," *IEEE Trans. on Magn.*, vol. **10**, pp. 123–127, 1974.
4) K. Honda, and S. Kaya: "On magnetization of single crystals of iron," *Sci. Rep. Tohoku Imp. Univ.*, vol. **15**, p. 721, 1926.

5) Nippon Steel Cat. No. SC 503 63.3, 1992.2.
6) S. Lopez, B. Cassoret, J. F. Brudny, L. Lefebvre, and J. N. Vincent: "Grain oriented steel assembly characterization for the development of high efficiency AC rotating electrical machines," *IEEE Trans. Magn.*, vol. **45**, no. 10, pp. 4161–4164, Oct. 2009.
7) S. Cicalé, L. Albini, F. Parasiliti, and M. Villani: "Design of a permanent magnet synchronous motor with grain oriented electrical steel for direct-drive elevators," in *Proc. XXth Int. Conf. Electrical Machines (ICEM)*, Marseille, 2012, pp. 1256–1263.
8) Y. Sugawara, and K. Akatsu: "Characteristics of a switched reluctance motor using grain-oriented electric steel sheet," in *Proc. Int. Conf. Electrical Machines and Systems (ICEMS)*, Busan, 2013, pp. 18–23.
9) Y. Enomoto, M. Kitamura, T. Sakai, and K. Ohara: "A way to select electrical sheets of the segment stator core motors," *IEEJ Trans. Ind. Appl.*, vol. **124**, no. 10, pp. 1010–1016, 2004. (in Japanese)
10) Y. Matsuo, T. Higuchi, T. Abe, Y. Miyamoto, and M. Ohto: "Characteristics of a novel segment type switched reluctance motor using grain-oriented electric steel," in *Proc. Int. Conf. Electrical Machines and Systems (ICEMS)*, Beijing, 2011, pp. 1–4.
11) S. Taghavi, and P. Pillay: "A novel grain-oriented lamination rotor core assembly for a synchronous reluctance traction motor with a reduced torque ripple algorithm," *IEEE Trans. Ind. Appl.*, vol. **52**, no. 5, pp. 3729-3738, Sep./Oct. 2016.
12) R. Koga, T. Todaka, and M. Enokizono: "Vector magnetic characteristic analysis of segment type synchronous reluctance motor utilizing grain-oriented electrical steel sheet," in *Proc. 15th Int. Conf. Electrical Machines and Systems (ICEMS)*, Sapporo, 2012, pp. 1–6.
13) J. Ma, R. Qu, and J. Li: "A novel axial flux switched reluctance motor with grain oriented electrical steel," in *Proc. IEEE Magn. Conf. (INTERMAG)*, Beijing, 2015, pp. 1-1.
14) K. Fujisaki, and K. Fujitani: "Design of stator core shape of 'magnetic anisotropic motor'," in *Proc. XXth Int. Conf. on Electrical Machines (ICEM)*, Marseille, 2012, pp. 183–189.
15) S. Takeda, K. Fujitani, S. Odawara, and K. Fujisaki: "Trial manufacture of magnetic anisotropic motor and evaluation of drag loss characteristics," in *Proc. Int. Conf. Electrical Machines (ICEM)*, Berlin, 2014, pp. 2055-2061.
16) H. Naumoski, B. Riedmüller, A. Minkow, and U. Herr: "Investigation of the influence of different cutting procedures on the global and local magnetic properties of non-oriented electrical steel," *J. of Magnetism and Magnetic Materials*, vol. **392**, pp. 126-133, Oct. 2015.
17) T. Kubota, M. Fujikura, M. Mizokami, and Y. Ushigami: "Electrical steel sheet for eco-design of electrical equipment," *Nippon Steel Technical Report*, no. 81, pp.53–57, Jan. 2000.
18) S. Aihara, H. Shimoji, T. Todaka, and M. Enokizono: "Measurement of local vector magnetic properties in laser scratched grain-oriented silicon steel sheet with vector-hysteresis sensor," *IEEE Trans. Magn.*, vol. **48**, no. 11, pp. 4499-4502, Nov. 2012.
19) A. Boglietti, P. Ferraris, M. Lazzari, and F. Profumo: "Iron losses in magnetic materials with six-step and PWM inverter supply [induction motors]," *IEEE Trans. Magn.*, vol. **27**, no. 6, pp.5334–5336, 1991.
20) N. Denis, K. Fujitani, Y. Kato, M. Ieki, and K. Fujisaki: "Core loss increase due to inverter carrier frequency in an interior permanent magnet synchronous motor," in *Proc. Int. Conf. Electrical Machines and Systems (ICEMS)*, Pattaya, 2015, pp. 1-7.
21) T. Nakata, and N. Takahashi: "Direct finite element analysis of flux and current distributions under specified conditions," *IEEE Trans. Magn.*, vol. **18**, no. 2, pp. 325-330, Mar 1982.
22) T. Tamaki, K. Fujisaki, K. Wajima, and K. Fujiwara: "Comparison of magnetic field analysis methods considering magnetic anisotropy," *IEEE Trans. Magn.,* vol. **46**, no.2, pp. 187–190, Feb. 2010.
23) L. Petrea, C. Demian, J. F. Brudny, and T. Belgrand: "High-frequency harmonic effects on low-frequency iron losses," *IEEE Trans. Magn.*, vol. **50**, pp. 1–4, Nov. 2014.
24) C. P. Steinmetz: "On the law of hysteresis," *Trans. Amer. Inst. Elec. Eng.*, vol. **IX**, no. 1, pp.1-64, Jan. 1892.
25) C. P. Steinmetz: "On the law of hysteresis (Part II.) and other phenomena of the magnetic circuit," *Trans. Amer. Inst. Elec. Eng.*, vol. **IX**, no. 1, pp. 619–758, Jan. 1892
26) K. Yamazaki, and H. Ishigami: "Rotor-shape optimization of interior-permanent-magnet motors to reduce harmonic iron losses," *IEEE Trans. Ind. Electro.*, vol. **57**, no. 1, pp. 61–69, Jan. 2010.
27) K. Yamazaki, and Y. Seto: "Iron loss analysis of interior permanent-magnet synchronous motors – variation of main loss factors due to driving condition," *IEEE Trans. Ind. Appl.*, vol. **42**, no. 4, pp. 1045–1052, Jul./Aug. 2006.
28) Y. Guo, J. G. Zhu, J. Zhong, H. Lu, and J. X. Jin: "Measurement and modeling of rotational core losses of soft magnetic materials used in electrical machines: A review," *IEEE Trans. on Magn.*, vol. **44**, no. 2, pp. 279-291, Feb. 2008.
29) S. Okamoto, N. Denis, Y. Kato, M. Ieki, and K. Fujisaki: "Core loss reduction of an interior permanent-magnet synchronous motor using amorphous stator core," *IEEE Trans. Ind. Appl.*, vol. **52**, no. 3, pp. 2261-2268, May/Jun. 2016.
30) K. Yamazaki, and A. Abe: "Loss investigation of interior permanent-magnet motors considering carrier harmonics and magnet eddy currents," *IEEE Trans. Ind. Appl.*, vol. **45**, no. 2, pp. 659-665, Mar./Apr. 2009.

Received Nov. 01, 2017; Accepted Mar. 27, 2018